Preprint Cambridge Centre for Computational Chemical Engineering ISSN 1473 – 4273

Improved methodology for performing the inverse Abel transform of flame images for colour ratio pyrometry

Jochen A.H. Dreyer[1,2], Radomir I. Slavchov[1], Eric J. Rees[1], Jethro Akroyd[1,2], Maurin Salamanca[1,2], Sebastian Mosbach[1,2], Markus Kraft[1,2,3]

released: 9 January 2018

[1] Department of Chemical Engineering
and Biotechnology
University of Cambridge
Philippa Fawcett Drive
Cambridge, CB3 0AS
United Kingdom

[2] Cambridge Centre for Advanced Research
and Education in Singapore (CARES)
CREATE Tower
1 Create Way
Singapore 138602

[3] School of Chemical
and Biomedical Engineering
Nanyang Technological University
62 Nanyang Drive
Singapore 637459
E-mail: mk306@cam.ac.uk

Preprint No. 217

Keywords: Colour ratio pyrometry, inverse Abel transformation, diffusion flame, soot, combustion

Edited by
Computational Modelling Group
Department of Chemical Engineering and Biotechnology
University of Cambridge
West Cambridge Site
Philippa Fawcett Drive
Cambridge CB3 0AS
United Kingdom

Fax: + 44 (0)1223 334796
E-Mail: c4e@cam.ac.uk
World Wide Web: http://como.cheng.cam.ac.uk/

Abstract

This letter reports a new regression method based on fitting the line-of-sight projection of a predefined intensity distribution (FLiPPID) to flame images for performing the Abel inversion. The aim is to develop a methodology that is less prone to experimental noise when analysing the projection of antisymmetric objects, in this case co-flow diffusion flame images for colour ratio pyrometry. A regression model is chosen for the light emission intensity distribution of the flame cross-section as a function of the radial distance from the flame centre-line. The forward Abel transform of this model function is fitted to the projected light intensity recorded by a colour camera. For each of the three colour channels, the model function requires three fitting parameters to match the radial intensity profile at each height above the burner. This results in a very smooth Abel inversion with no artefacts such as oscillations or negative values of the light source intensity, as is commonly observed for alternative Abel inversion techniques, such as the basis-set expansion (BASEX) or onion-peeling. The advantages of the new FLiPPID method are illustrated by calculating the soot temperature and volume fraction profiles inside a co-flow diffusion flame, both being significantly smoother than those produced by the alternative inversion methods.

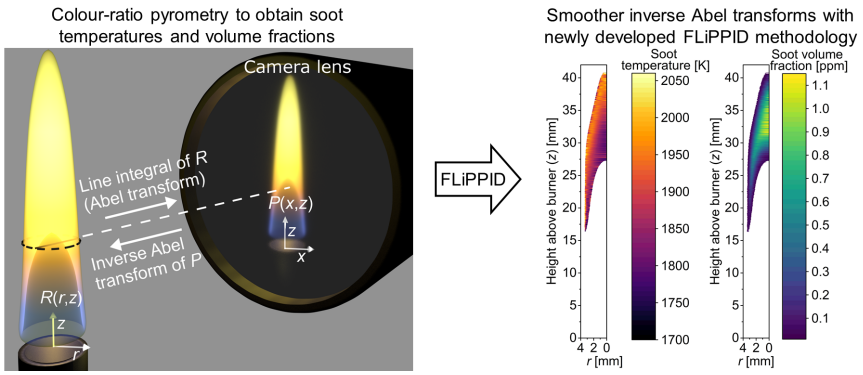

Highlights

- New regression based methodology (FLiPPID) for performing the inverse Abel transform is reported.
- FLiPPID results in smoother cross-section profiles of the soot temperature and volume fraction obtained from colour-ratio pyrometry experiments.
- Methodology applicable in other experimental techniques where the 2D projection of asymmetric, optically thin objects is recorded.

Contents

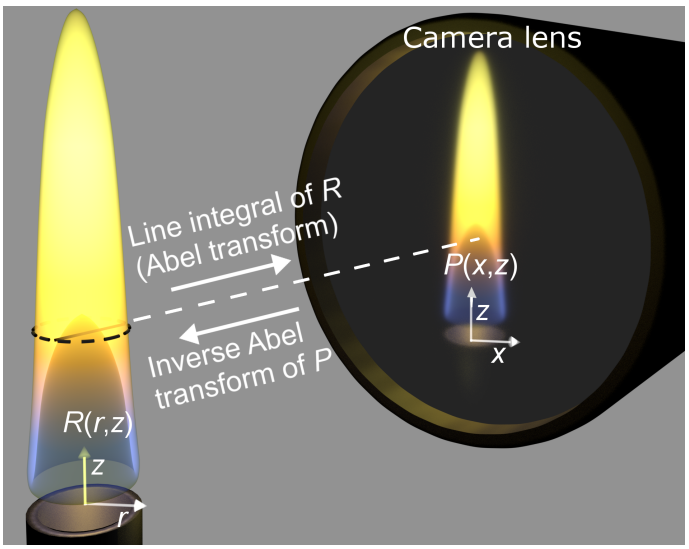

Figure 1: *Illustration of the relationship between the original light emission distribution $R(r,z)$ of the flame cross-section and its projection $P(x,z)$.*

1 Introduction

Laminar flames are widely used for fundamental studies of soot formation [1, 6, 32, 34] and the synthesis of materials [12, 29, 33]. Characterising such systems with accurate and reliable techniques is vital for understanding the processes controlling particle formation in flames and is an ongoing field of research [18]. The employed techniques can generally be divided into intrusive and non-intrusive methods. Examples for the former are measurements of the flame temperature with a thermocouple, soot sampling to measure particle size distributions [1, 30], or thermophoretic soot collection for *ex situ* analysis [3, 4]. Whenever possible, non-intrusive techniques are preferred to avoid perturbation of the system. One such technique that has gained increasing attention in recent years, is colour ratio pyrometry [7, 9, 16, 18]. Here, the intensity and colour of the visible light emitted by hot soot are used to infer their temperature and volume fraction [21, 24]. No expensive equipment is required, making pyrometry an economic and rapid method to obtain 2D soot temperature and volume fraction data.

One of the main challenges in colour ratio pyrometry is the reconstruction of the flame cross-section emission profile, $R(r,z)$, from the projected area profile $P(x,z)$ recorded by a camera (Fig. 1). In case of optically thin flames (i.e. negligible soot self-absorption [18]) with axial symmetry, the recorded 2D projection $P(x,z)$ and the 3D flame emission density $R(r,z)$ are linked through the forward and reverse Abel transforms [2, 10, 11, 14]:

$$P(x,z) = 2\int_x^\infty \frac{R(r,z)r}{\sqrt{r^2-x^2}}\mathrm{d}r, \tag{1}$$

$$R(r,z) = -\frac{1}{\pi}\int_r^\infty \frac{\partial P(x,z)}{\partial x}\frac{1}{\sqrt{x^2-r^2}}\mathrm{d}x, \tag{2}$$

where z is the height above the burner (HAB), r is the cylindrical coordinate and x is the projected coordinate (distance from the central axis).

Unfortunately, applying the inverse transform directly to experimental data recorded for P is not feasible because it significantly amplifies the experimental noise, especially close to the axis of symmetry [20]. Numerous methods have been developed to circumvent this issue and to reduce the noise amplification upon image reconstruction. Two techniques commonly used for flame pyrometry are the basis-set expansion (BASEX) [2, 14] and the onion-peeling method combined with a Tikhonov regularisation [10, 11]. These approaches are similar in that they both use regularisation (smoothing and filtering) parameters to reduce the experimental noise. Whilst these methods are computationally cheap, both of them still tend to amplify the noise in $R(r,z)$, especially close to the axis of symmetry. The noisy image reconstruction has a significant effect on the soot temperatures T and volume fractions f_v computed from R. This is especially problematic if flame centre-line values are the desired quantity. For example, estimating sooting propensities of fuels with the yield sooting indices (YSIs) requires the maximum of f_v, which is often in the flame centre [7, 27, 28].

The **purpose of this letter** is to describe a new Abel inversion technique that is less sensitive to noise and allows the reconstructions of smooth intensity cross-sections from their 2D projections. The proposed method is based on fitting the line-of-sight projection of a predefined intensity distribution (FLiPPID) to the recorded projection. The predefined intensity distribution $R(r)$ has to be tailored to the geometry of the studied signal source. However, the methodology is general and can be applied to any steady, optically thin, axisymmetric system.

2 Experiments

The system studied here was a co-flow diffusion flame. The analysed signal originated from hot soot particles emitting black body radiation (Fig. 1). The flame was stabilised using a Yale burner [26] fed with 7 g/h pre-vaporised (Bronkhorst CEM) *n*-heptane in 200 mL/min argon carrier gas. The fuel/carrier gas mixture was delivered through heated lines to a central 1/4" stainless steel tube (inner diameter 0.218"). A 50 L/min co-flow of air were passed through a 3" honeycomb mesh (0.017" wire diameter, 18x18 mesh). Images of the flame were recorded in a raw format using a Blackfly S colour camera (FLIR Integrated Imaging Solutions) with a CMOS sensor (2048 x 1536 pixels). A BG-7 filter (Thorlabs) was used to balance the intensity ratios of the three colour channels and to block infra-red light. The image processing was performed on a single image frame to avoid blurring of the flame edges. A more detailed description of the steps involved in processing the image as well as an algorithm flow chart (Fig. S1) is given in the Supporting information.

3 FLiPPID Methodology

The FLiPPID method developed here requires the definition of a suitable function $R(r;a,b,c...)$, $a,b,c...$ being fitting parameters, that is able to describe the intensity distribution at the cross-section of the studied signal source. The forward Abel transform (Eq. 1) of R was computed numerically to obtain $P(x;a,b,c...)$. A sum-of-squares objective function $g(z;a,b,c,...)$ describing the difference between the calculated projection P and the corresponding experimentally recorded 2D projection was minimised using a Simplex optimisation. The fitting procedure was repeated for all pixel rows in z and thus all height above the burner (HAB), as well as for each of the three colour channels. Further details and an algorithm flow chart are provided in the Supporting Information (Fig. S2 and S3).

To aid finding a suitable model function $R(r;a,b,c...)$, the following criteria were defined: (i) R must be positive at all r; and (ii) R should be applicable to cross-sections at all z. In the case of the diffusion flame studied here, two additional requirements were that (iii) R decays exponentially or faster at large r; and (iv) depending on the fitting parameters, $R(r)$ has either a single maximum at $r = 0$ or two symmetric maxima plus a local minimum at $r = 0$. (v) The agreement between a function R and the data was considered sufficiently good when the optimal value of the objective function g was no more than 0.5% different from the intrinsic sum of squares of the experimental data, g_{int}. The latter parameter was defined as the minimal value of the sum of squares for the recorded data at a given z and a set of models for P generated by fitting polymonials of increasing order n to the data. The optimal sum of squares of the polynomial models decreased with n until a well-defined plateau value - namely, g_{int} - was reached at n=15–30. The optimal sum of squares for the polynomial models does not decrease further until n approaches the number of data points, producing oscillating polynomial functions following the noise of the measured data.

The plateau value g_{int} is a practically model-independent characteristic of the recorded data, and is used as a benchmark for how well a model can possibly fit the data.

4 Results

A function $R(r;a,b,c)$ that fulfils all of the above requirements (i)-(v) is:

$$R(r) = \frac{a}{b\sqrt{\pi}}\exp[c(\frac{r}{b})^2 - (\frac{r}{b})^6], \quad a,b \in \mathbb{R}^+, \quad c \in \mathbb{R} \tag{3}$$

Here, a is characteristic of the amplitude of R, b is of the order of magnitude as the radius of the flame, and c defines the position of the two extrema in the lower part of the flame. No other 4-, 5- or 6-parameter test function for R was found that led to a g significantly closer to g_{int} than the one given by Eq. 3.

Fig. 2(a) compares flame projections at two HAB, recorded by the green channel, with the corresponding fits of Eqs. 3 and its forward Abel transform (Eq. 1). Excellent agreement between the fitted and recorded data was obtained despite the simplicity of the regression

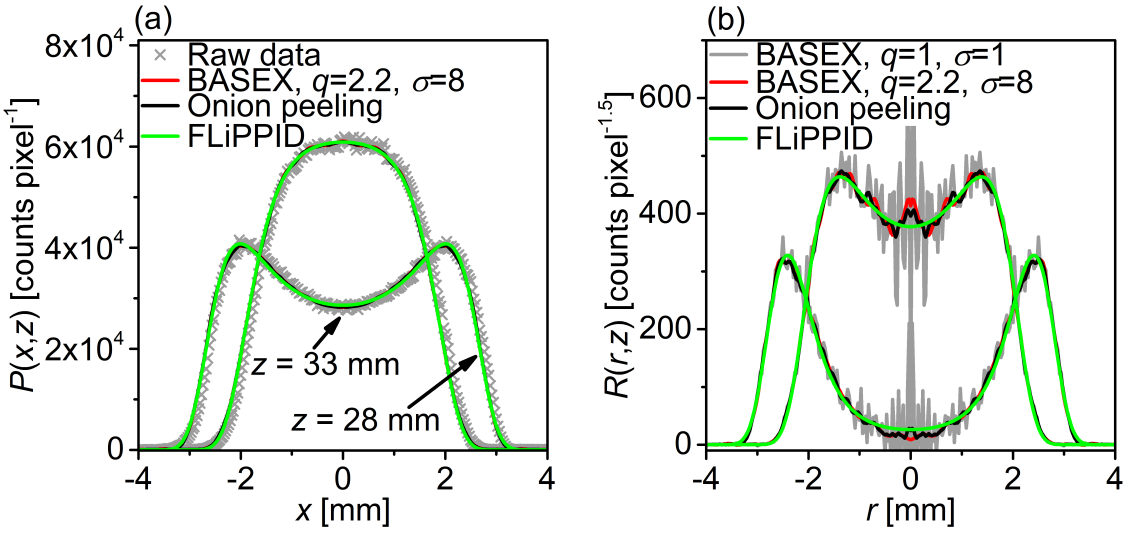

Figure 2: *(a) Recorded green light projection of the flame at z = 33 and 28 mm (highlighted in Fig. 3(a)) together with FLiPPID and smoothed/filtered $P(x)$ using BASEX and onion peeling. (b) Reconstructed cross-section density from the data in (a) using the three different methods as well as BASEX without smoothing/filtration ($q = 1, \sigma = 1$).*

model and the diverse profile shapes at different HAB. Fits at other z and for other colour channels led to equally good or better results (the projection for z = 28 mm led to the worst fit).

Two state-of-the-art techniques frequently used for the inverse Abel transform of flame images, BASEX [9, 14] and onion peeling with Tikhonov regularisation [10, 18]), were compared to the FLiPPID method. The regularisation parameters for the former two methods were chosen such that significant smoothing of the reconstructed R was achieved while avoiding large oscillations. The results for BASEX without any smoothing/filtering ($q = 1, \sigma = 1$) are also shown in Fig. 2(b). For BASEX with $q = 2.2, \sigma = 8$ and the onion-peeling technique, the smoothed/filtered $P(x,z)$ are hardly distinguishable from FLiPPID (Fig. 2(a)). However, both BASEX and onion peeling led to substantial noise in R, especially close to the flame centre (Fig. 2(b)). In contrast, Eq. 3 of FLiPPID is by definition a smooth function, including close to the axis of symmetry. It should be noted that in terms of computational time, the fitting approach of FLiPPID can not compete with the fast matrix operations of BASEX and onion-peeling. However, once an appropriate function for R is chosen, FLiPPID can be easily accelerated by tabulating the Abel transform of R (Eq. 1) and the results are of higher quality than for the more rapid methods.

It is worth mentioning that fitting a function directly to $P(x)$ followed by the inverse transform (Eq 2) was also attempted but proofed to be impractical. Not even 10-parameter models for P matched the performance of the FLiPPID method, in terms of g and applicability to any HAB. Besides, fitting a function to P proved to be as problematic as the BASEX and onion-peeling techniques, sometimes causing oscillations in R or even non-physical, negative values of R near the central axis. The FLiPPID method *a priori*

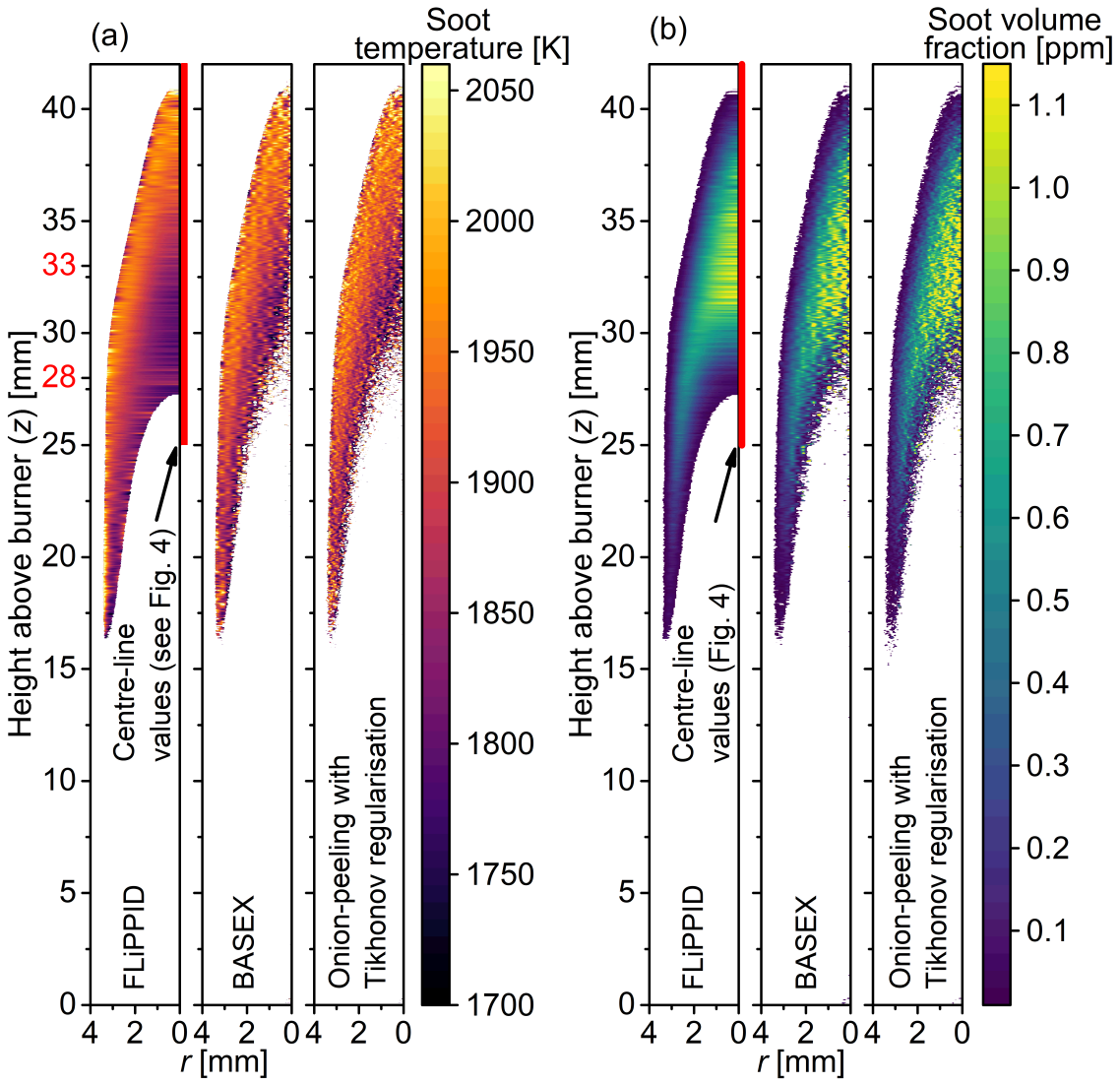

Figure 3: *Calculated (a) soot temperature T and (b) volume fraction f_v (b) using three different methods for performing the inverse Abel transform (see bottom labels). For 28 mm and 33 mm HAB, line plots of the intensity recorded with the green camera channel are plotted in Fig. 2. The distributions of T and f_v over the highlighted centre-lines values of (a) and (b) are shown in Fig. 4.*

assumes a positive, smooth density and, therefore, does not suffer from such artefacts.

Once the emission source densities $R(r,z)$ are known for the three colour channels, the soot temperature T can be computed. The relationship between the recorded colour ratio and the T of the light-emitting incandescent material is given by [21]:

$$\frac{R_i}{R_j} = \frac{\int_0^\infty \eta_i(\lambda)\frac{\varepsilon(\lambda)}{\lambda^5}[\exp(hc/\lambda kT)-1]^{-1}\mathrm{d}\lambda}{\int_0^\infty \eta_j(\lambda)\frac{\varepsilon(\lambda)}{\lambda^5}[\exp(hc/\lambda kT)-1]^{-1}\mathrm{d}\lambda}, \tag{4}$$

where λ is the wavelength, k and h are the Boltzmann and Planck constants, c is the speed of light, and $\varepsilon(\lambda)$ is the material's emissivity. R_i and $\eta_i(\lambda)$ are the reconstructed intensity and the camera response of the colour channel i. $\eta_i(\lambda)$ was obtained using the quantum efficiency of the camera and wavelength dependent filter transmission data provided by the respective manufacturers. For calibration, an R-type thermocouple was placed at different distances above a Bunsen burner and imaged. The detected colour ratios at different thermocouple temperatures (1570-1930 K) were used to calibrate the camera response [21]. For $\varepsilon(\lambda)$ of the thermocouple, the emissivity values reported by Ma and Long [24] were used. Using the calibrated camera response in Eq. 4 (see Supporting Information for more details), the expected light colour of soot was calculated as a function of temperature. The results of the calculations were used to create a look-up table for the temperature as a function of the three different RGB ratios (Fig. S4). Assigning a value of $\varepsilon(\lambda)$ for soot is not straightforward as it is a function of the soot growth history and carbon/hydrogen ratio, and thus varies within the flame [13, 19, 23, 25]. The optical properties of soot are beyond the scope of this letter and the most commonly used dependence in the field [7, 13, 21], $\varepsilon(\lambda) \propto \lambda^{-1.38}$, was used.

Fig. 3(a) compares the calculated soot temperatures using FLiPPID, BASEX and onion-peeling for converting the recorded projected intensity profiles $P(x,z)$ to the emission intensity cross-section distributions $R(r,z)$. The shown temperatures were obtained using Eq. 4, with three different RGB ratios (R/G, R/B, G/B) and averaging the results as per [21]. The regularisation parameters for the BASEX and Tikhonov regularisation were the same as used in Fig. 2. All the other conditions (assumed $\varepsilon(\lambda)$ for soot, raw flame image, the T look-up table) were identical. The soot temperatures are in a similar range as the ones reported for similar co-flow diffusion flames using different fuels [7, 21]. All three methods (FLiPPID, BASEX, onion-peeling with Tikhonov regularisation) gave qualitatively similar temperature distributions. However, BASEX and onion-peeling both gave noisy results close to the centre-line. Below 32 mm HAB, the centre-line temperatures were too noisy to obtain reliable values. FLiPPID led to relatively smooth centre-line temperatures even down to 27 mm HAB. The reduction in noise along the flame centre is further illustrated in Fig. 4(a).

Once T is known, the soot volume fraction f_v can be calculated [5, 21, 24]:

$$f_\mathrm{v} = -\frac{\lambda_\mathrm{eff}}{K_\mathrm{ext} L} \ln\left(1 - \varepsilon_\mathrm{L}(\lambda_\mathrm{eff}) \frac{R_\mathrm{i}}{S_\mathrm{L}}\right) \approx \frac{\lambda_\mathrm{eff} \varepsilon_\mathrm{L}}{K_\mathrm{ext} L} \frac{R_\mathrm{i}}{S_\mathrm{L}} \tag{5}$$

(as it follows from Eqs. 1&5 of Ref. [5]; the expansion of the natural logarithm in series is accurate for optically thin flames). Here, λ_eff is the effective filter wavelength [24], K_ext is the soot dimensionless extinction coefficient (value taken as 8.6 [21]), L is the pixel dimension (1 mm per 34 pixels), and $\varepsilon_\mathrm{L}(\lambda_\mathrm{eff})$ is the emissivity at λ_eff of the calibration source (R-type thermocouple). The light emitted from a layer of soot particles, 1 pixel thick, which is recorded by colour channel i is R_i. For R_i, the intensity of the green colour channel obtained by applying FLiPPID, BASEX, or onion-peeling was used. Images of the hot thermocouple provided the light intensity of the calibration source (S_L, see Fig. S5). An interpolation of S_L as a function of the temperature was used in Eq. 5 at the respective soot temperature calculated previously (Fig. 3(a)).

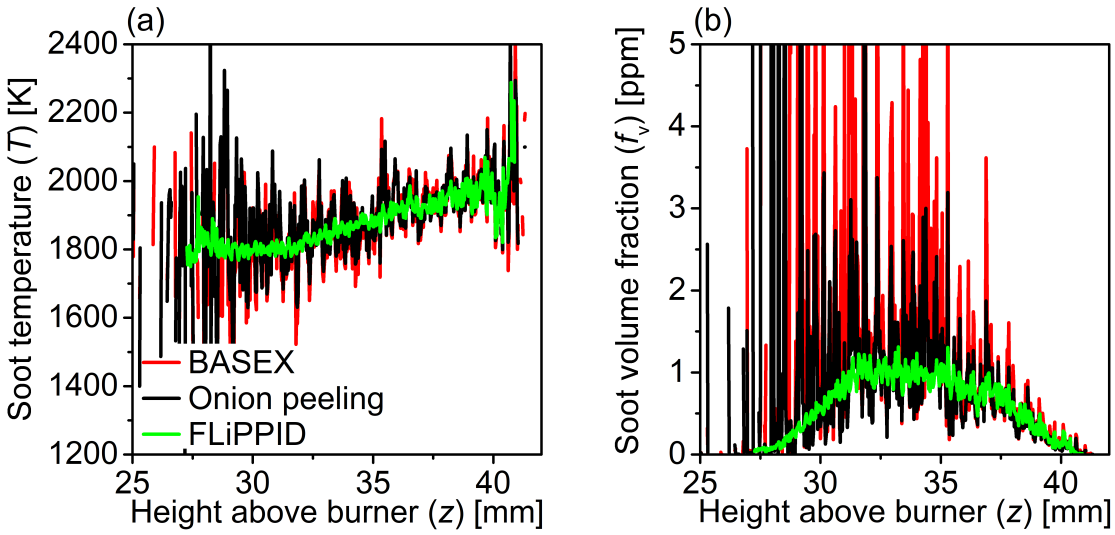

Figure 4: *Flame centre-line values for the soot temperature (a) and volume fractions (b) using three different methods for performing the inverse Abel transform.*

The values of f_v calculated using the three Abel inversion methods are shown in Fig. 3(b). The maximum value of f_v was around 1.1 ppm, which is in between values reported for co-flow diffusion flames fed with methane (0.08 ppm [7, 8]) and ethylene (5-8 ppm [13, 21]) and similar to a nitrogen diluted *n*-heptane operated at 2 bar (0.8 ppm) [17]. Among the three methods for Abel inversion, the new FLiPPID method led to significantly smoother profiles. This is evident on the plot of the centre-line values of f_v against HAB (Fig. 4(b)). Note that for FLiPPID, single pixel centre-line values are shown in Fig. 4 while for BASEX and onion-peeling, averages of the central 11 pixels (corresponding to 0.32 mm) were used instead to reduce the noise. Even then, the values obtained with BASEX and onion peeling were significantly noisier.

5 Conclusions

In conclusion, the newly developed FLiPPID method enabled smooth reconstruction of flame cross-sections, even close to the flame centre-line. The obtained values for the soot temperature T and volume fraction f_v were generally in a similar range as for commonly used Abel inversion methods (BASEX and onion peeling with Tikhonov regularisation). However, FLiPPID produced significantly less noisy reconstructed images compared to BASEX and onion-peeling, especially close to the flame centre. The predefined intensity distribution chosen here (Eq. 3) was optimised for co-flow diffusion flames and preliminary tests showed that Eq. 3 seems to be applicable to a wide range of co-flow diffusion flames. It is expected that the FLiPPID methodology described here can also be applied to other experimental techniques employing the Abel transform (e.g., modulated absorption/emission [15, 22] or in-line holography [2, 31]) simply by adjusting or extending (Eq. 3).

Acknowledgements

This project is funded by the National Research Foundation, Prime Minister's Office, Singapore under its CREATE programme.

References

[1] A. D. Abid, J. Camacho, D. A. Sheen, and H. Wang. Quantitative measurement of soot particle size distribution in premixed flames - The burner-stabilized stagnation flame approach. *Combust. Flame*, 156:1862–1870, 2009. doi:10.1016/j.combustflame.2009.05.010.

[2] M. Apostolopoulos, M. Taroudakis, and D. Papazoglou. Application of inverse Abel techniques in in-line holographic microscopy. *Opt. Commun.*, 296:25–34, 2013. doi:10.1016/J.OPTCOM.2013.01.053.

[3] M. L. Botero, N. Eaves, J. A. Dreyer, Y. Sheng, J. Akroyd, W. Yang, and M. Kraft. Experimental and numerical study of the evolution of soot primary particles in a diffusion flame. *Proc. Combust. Inst.*, 2018. doi:10.1016/J.PROCI.2018.06.185.

[4] M. L. Botero, Y. Sheng, J. Akroyd, J. Martin, J. A. Dreyer, W. Yang, and M. Kraft. Internal structure of soot particles in a diffusion flame. *Carbon*, 141:635–642, 2019. doi:10.1016/J.CARBON.2018.09.063.

[5] F. Cignoli, S. De Iuliis, V. Manta, and G. Zizak. Two-dimensional two-wavelength emission technique for soot diagnostics. *Appl. Opt.*, 40:5370–5378, 2001. doi:10.1364/AO.40.005370.

[6] M. Conturso, M. Sirignano, and A. D'Anna. Effect of C_9H_{12} alkylbenzenes on particle formation in diffusion flames: An experimental study. *Fuel*, 191:204–211, 2017. doi:http://dx.doi.org/10.1016/j.fuel.2016.11.050.

[7] D. D. Das, W. J. Cannella, C. S. McEnally, C. J. Mueller, and L. D. Pfefferle. Two-dimensional soot volume fraction measurements in flames doped with large hydrocarbons. *Proc. Combust. Inst.*, 36:871–879, 2017. doi:10.1016/j.proci.2016.06.047.

[8] D. D. Das, C. S. McEnally, T. A. Kwan, J. B. Zimmerman, W. J. Cannella, C. J. Mueller, and L. D. Pfefferle. Sooting tendencies of diesel fuels, jet fuels, and their surrogates in diffusion flames. *Fuel*, 197:445–458, 2017. doi:10.1016/J.FUEL.2017.01.099.

[9] D. D. Das, P. C. St. John, C. S. McEnally, S. Kim, and L. D. Pfefferle. Measuring and predicting sooting tendencies of oxygenates, alkanes, alkenes, cycloalkanes, and aromatics on a unified scale. *Combust. Flame*, 190:349–364, 2018. doi:10.1016/J.COMBUSTFLAME.2017.12.005.

[10] C. J. Dasch. One-dimensional tomography: A comparison of Abel, onion-peeling, and filtered backprojection methods. *Appl. Opt.*, 31:1146, 1992. doi:10.1364/AO.31.001146.

[11] K. J. Daun, K. A. Thomson, F. Liu, and G. J. Smallwood. Deconvolution of axisymmetric flame properties using Tikhonov regularization. *Appl. Opt.*, 45:4638, 2006. doi:10.1364/AO.45.004638.

[12] G. De Falco, A. Porta, A. M. Petrone, P. Del Gaudio, A. El Hassanin, M. Commodo, P. Minutolo, A. Squillace, and A. D'Anna. Antimicrobial activity of flame-synthesized nano-TiO_2 coatings. *Environ. Sci.: Nano*, 4:1095–1107, 2017. doi:10.1039/C7EN00030H.

[13] S. De Iuliis, M. Barbini, S. Benecchi, F. Cignoli, and G. Zizak. Determination of the soot volume fraction in an ethylene diffusion flame by multiwavelength analysis of soot radiation. *Combust. Flame*, 115:253–261, 1998. doi:10.1016/S0010-2180(97)00357-X.

[14] V. Dribinski, A. Ossadtchi, V. A. Mandelshtam, and H. Reisler. Reconstruction of Abel-transformable images: The Gaussian basis-set expansion Abel transform method. *Rev. Sci. Instrum.*, 73:2634–2642, 2002. doi:10.1063/1.1482156.

[15] B. Franzelli, M. Roussillo, P. Scouflaire, J. Bonnety, R. Jalain, T. Dormieux, S. Candel, and G. Legros. Multi-diagnostic soot measurements in a laminar diffusion flame to assess the ISF database consistency. *Proc. Combust. Inst.*, 2018. doi:10.1016/j.proci.2018.05.062.

[16] H. Guo, J. A. Castillo, and P. B. Sunderland. Digital camera measurements of soot temperature and soot volume fraction in axisymmetric flames. *Appl. Opt.*, 52:8040, 2013. doi:10.1364/AO.52.008040.

[17] A. E. Karataş, G. Intasopa, and Ö. L. Gülder. Sooting behaviour of *n*-heptane laminar diffusion flames at high pressures. *Combust. Flame*, 160(9):1650–1656, 2013. doi:10.1016/J.COMBUSTFLAME.2013.03.008.

[18] N. J. Kempema and M. B. Long. Effect of soot self-absorption on color-ratio pyrometry in laminar coflow diffusion flames. *Opt. Lett.*, 43:1103, 2018. doi:10.1364/OL.43.001103.

[19] N. J. Kempema, B. Ma, and M. B. Long. Investigation of in-flame soot optical properties in laminar coflow diffusion flames using thermophoretic particle sampling and spectral light extinction. *Appl. Phys. B*, 122:232, 2016. doi:10.1007/s00340-016-6509-6.

[20] P. S. Kolhe and A. K. Agrawal. Abel inversion of deflectometric data: comparison of accuracy and noise propagation of existing techniques. *Appl. Opt.*, 48:3894, 2009. doi:10.1364/AO.48.003894.

[21] P. B. Kuhn, B. Ma, B. C. Connelly, M. D. Smooke, and M. B. Long. Soot and thin-filament pyrometry using a color digital camera. *Proc. Combust. Inst.*, 33:743–750, 2011. doi:10.1016/j.proci.2010.05.006.

[22] G. Legros, Q. Wang, J. Bonnety, M. Kashif, C. Morin, J.-L. Consalvi, and F. Liu. Simultaneous soot temperature and volume fraction measurements in axis-symmetric flames by a two-dimensional modulated absorption/emission technique. *Combust. Flame*, 162:2705–2719, 2015. doi:10.1016/j.combustflame.2015.04.006.

[23] F. Liu, K. A. Thomson, and G. J. Smallwood. Soot temperature and volume fraction retrieval from spectrally resolved flame emission measurement in laminar axisymmetric coflow diffusion flames: Effect of self-absorption. *Combust. Flame*, 160: 1693–1705, 2013. doi:10.1016/J.COMBUSTFLAME.2013.02.007.

[24] B. Ma and M. B. Long. Absolute light calibration using S-type thermocouples. *Proc. Combust. Inst.*, 34(2):3531–3539, 2013. doi:10.1016/j.proci.2012.05.030.

[25] B. Ma and M. B. Long. Combined soot optical characterization using 2-D multi-angle light scattering and spectrally resolved line-of-sight attenuation and its implication on soot color-ratio pyrometry. *Appl. Phys. B*, 117:287–303, 2014. doi:10.1007/s00340-014-5834-x.

[26] C. McEnally, A. Schaffer, M. Long, L. Pfefferle, M. Smooke, M. Colket, and R. Hall. Computational and experimental study of soot formation in a coflow, laminar ethylene diffusion flame. *Proc. Combust. Inst.*, 27:1497–1505, 1998. doi:10.1016/S0082-0784(98)80557-2.

[27] C. S. McEnally and L. D. Pfefferle. Improved sooting tendency measurements for aromatic hydrocarbons and their implications for naphthalene formation pathways. *Combust. Flame*, 148:210–222, 2007. doi:10.1016/J.COMBUSTFLAME.2006.11.003.

[28] C. S. McEnally and L. D. Pfefferle. Sooting tendencies of oxygenated hydrocarbons in laboratory-scale flames. *Environ. Sci. Technol.*, 45:2498–2503, 2011. doi:10.1021/es103733q.

[29] N. K. Memon, F. Xu, G. Sun, S. J. B. Dunham, B. H. Kear, and S. D. Tse. Flame synthesis of carbon nanotubes and few-layer graphene on metal-oxide spinel powders. *Carbon*, 63:478–486, 2013. doi:10.1016/j.carbon.2013.07.023.

[30] A. Naseri, A. Veshkini, and M. J. Thomson. Detailed modeling of CO_2 addition effects on the evolution of soot particle size distribution functions in premixed laminar ethylene flames. *Combust. Flame*, 183:75–87, 2017. doi:10.1016/j.combustflame.2017.04.028.

[31] D. G. Papazoglou and S. Tzortzakis. In-line holography for the characterization of ultrafast laser filamentation in transparent media. *Appl. Phys. Lett.*, 93(4):041120, 2008. doi:10.1063/1.2968190.

[32] Y. R. Tan, M. L. Botero, Y. Sheng, J. A. H. Dreyer, R. Xu, W. Yang, and M. Kraft. Sooting characteristics of polyoxymethylene dimethyl ether blends with diesel in a diffusion flame. *Fuel*, 224:499–506, 2018. doi:10.1016/j.fuel.2018.03.051.

[33] E. D. Tolmachoff, A. D. Abid, D. J. Phares, C. S. Campbell, and H. Wang. Synthesis of nano-phase TiO_2 crystalline films over premixed stagnation flames. *Proc. Combust. Inst.*, 32:1839–1845, 2009. doi:10.1016/j.proci.2008.06.052.

[34] T. Zhang, L. Zhao, and M. J. Thomson. Effects of *n*-propylbenzene addition to *n*-dodecane on soot formation and aggregate structure in a laminar coflow diffusion flame. *Proc. Combust. Inst.*, 36:1339–1347, 2017. doi:10.1016/j.proci.2016.05.026.

A Supporting Information

Image processing

The Matlab code for calculating soot temperature and volume fraction profiles is schematically shown in Fig. S1. A brief description of each step is given below.

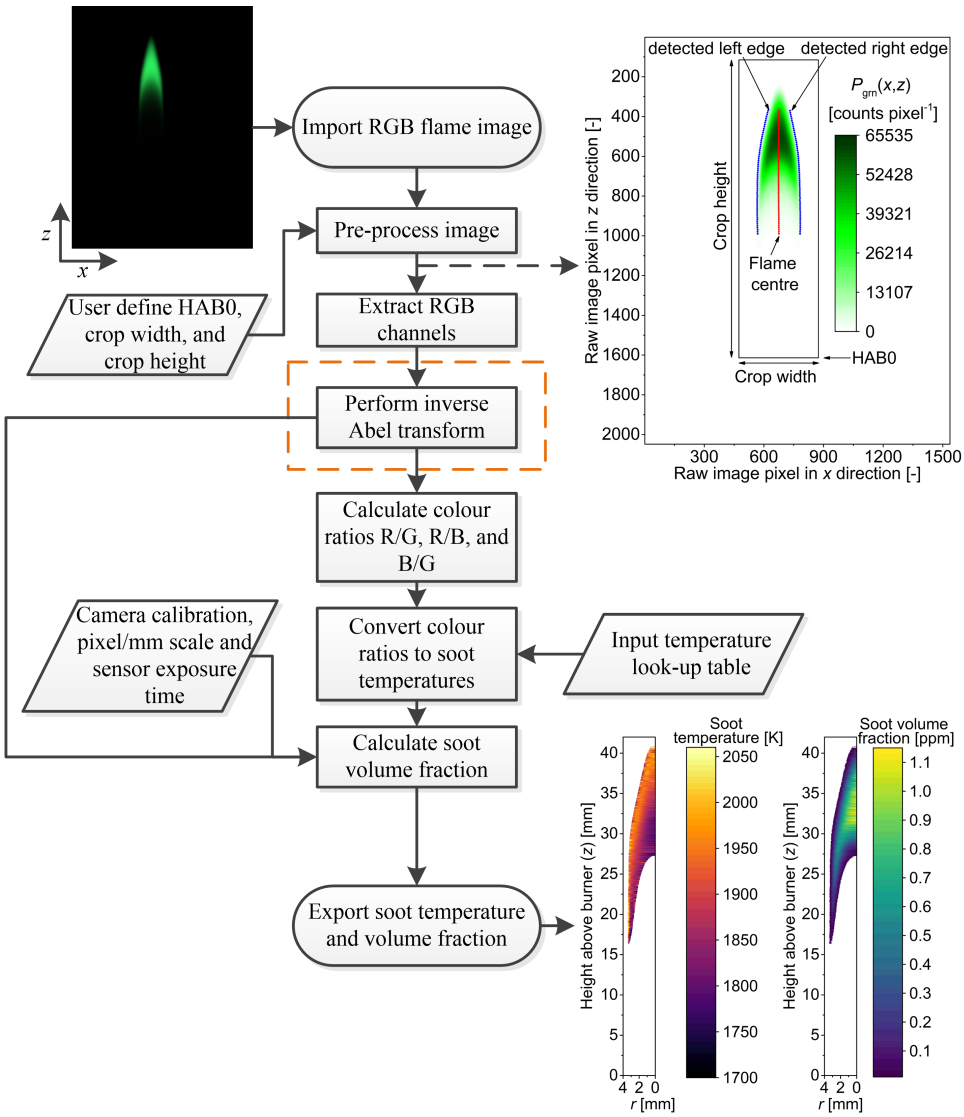

Figure S1: *Algorithm flow chart for converting the recorded RGB flame image to cross-section profiles of the soot temperature and volume fraction*

Import RGB flame image The images were recorded in 12 bit raw format with a resolution of 1536x2048 pixel. The images were converted to tif format using ImageJ and imported into Matlab. The RGB channels are obtained by debayering the raw image with Matlab's `demosaic` function.

Pre-process image For performing the inverse Abel transform, the flame image has to be cropped such that the axis of symmetry is in the centre. The Matlab code automatically detects the flame edges by searching for the first and last column above a threshold and taking the middle of these as centre (Fig. S1). The procedure is repeated for a number of rows to obtain an averaged flame centre and to check that the flame is not tilted. The user-defined burner position (HAB0), crop width and crop height are used to cut the raw image from HAB0 to crop height in z-direction and to the crop width with the flame centre in the middle in x-direction (see Fig. S1).

Extract RGB channels The cropped red, green, and blue colour channels of the image are extracted.

Performing inverse Abel transform The inverse Abel transform of the image is calculated for each colour channel. The detailed flow chart of the newly developed FLiPPID method is shown in Fig. S2 and described below. Alternative methods such as the basis-set expansion (BASEX) [2, 14] and the onion-peeling method combined with a Tikhonov regularisation [10, 11] are described in detail in the literature.

Calculate colour ratios R/G, R/B, and B/G The colour ratios of the reconstructed flame cross sections are calculated. If the intensity of one of the colour channels falls below a predefined threshold, the ratio at this pixel is set to 0 to prevent meaningless background colour ratios to be calculated.

Convert colour ratios to soot temperatures The calculated colour ratios are converted to soot temperatures using a temperature look-up table (Fig. S4). A description of how this table is obtained is given below.

Calculate soot volume fraction Using Eq. 5, the previously obtained soot temperatures, the camera exposure time used while recording the flame image, and the camera calibration (Fig. S5), the soot volume fractions are calculated.

Export soot temperature and volume fraction The obtained soot temperature and volume fraction profiles are exported.

FLiPPID

Import pre-processed RGB channels Input to the FLiPPID method are matrices of the experimental 2-D projections recorded by the camera and the predefined intensity distribution $R(r; a, b, c)$ (Eq. 3 in this study). The axis of symmetry of the experimental data has to be in the centre of the matrix.

Select first colour channel i The first RGB colour channel is selected, i.e., i is set to red, green, or blue.

Initial guess for a, b, c The initial values for a, b, c are provided by the user. The values should be reasonable to assure fast convergence in the subsequent optimisation. For $R(r; a, b, c)$ used here (Eq. 3), $a/b\sqrt{\pi}$ is the intensity at r=0, b is of the order of the flame radius, and c determines the radial position of the maximum intensity. The optimised values of a, b, c obtained for the green colour channel are plotted in Fig. S3 to facilitate the selection of initial guesses.

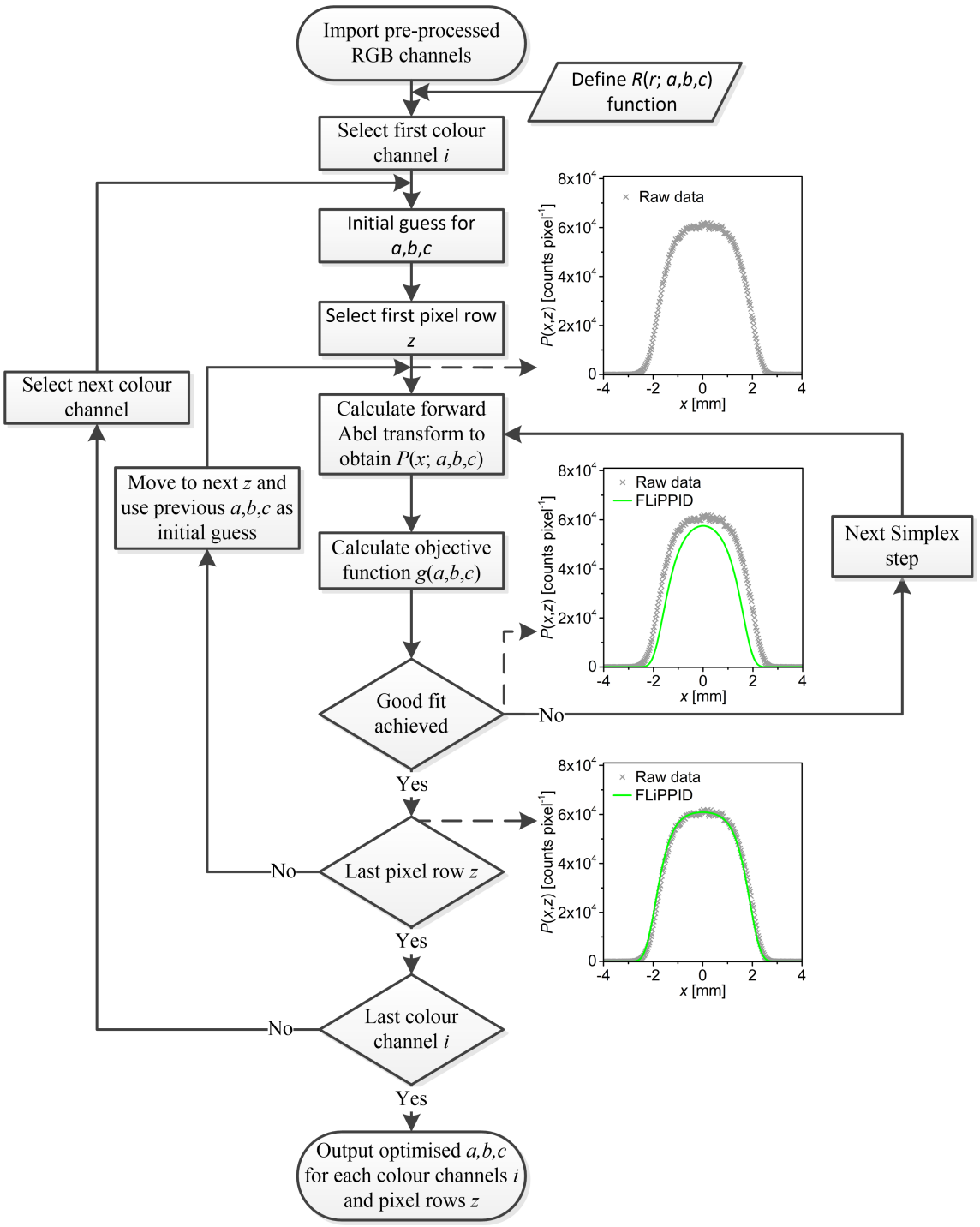

Figure S2: *Algorithm flow chart of the FLiPPID method on the example of RGB flame images.*

Calculate froward Abel transform to obtain $P(x; a, b, c)$ The line-of-sight projection of $R(r; a, b, c)$ is calculated using the forward Abel transform (Eq. 1). This is the computationally most time-consuming step of the FLiPPID method.

Compare experimental data of colour channel i at pixel row z to $P(x; a,b,c)$ A sum-of-squares objective function $g(z;a,b,c,...)$ describing the difference between the calculated projection P and the corresponding experimentally recorded 2D projection P_{exp} is calculated to quantify the difference between them:

$$g = \frac{1}{x_{\max}} \sum_{n=1}^{x_{\max}} [P(x_n) - P_{\text{exp}}(x_n)]^2$$

Good fit achieved The algorithm checks if a good fit was achieved between the experimental raw data and the $P(x;\ a,b,c)$. The applied stop condition is that, within a user-defined number of iterations steps, g does not decrease by more than a user-defined margin.

Next Simplex step The next set of values for a,b,c are selected according to the Simplex algorithm.

Last pixel row z If the last pixel row z of the input matrix was reached, the code checks if there are other colour channels to process. If the last z was not reached the next pixel row is selected and the previously optimised a,b,c are used as initial guess. It is worth noting that more than one minimum in g was observed for some flame regions. In order to detect other minima and to assure the global minimum was found, several random sets of initial values for a,b,c were chosen every few steps of z.

Last colour channel If all three RGB channels were processed, the programme exits. Otherwise the next colour channel is selected.

Output optimised a,b,c for each colour channel i and pixel row z Matrices of a,b,c for the three colour channels as function of z are exported. An example for the optimised parameters of the green colour channel is shown in Fig. S3.

Camera calibration

Temperature look-up table The colour ratios that would be expected to be recorded when photographing a hot object can be calculated using Eq. 4 of the main manuscript:

$$\frac{R_i}{R_j} = \frac{\int_0^\infty \eta_i(\lambda) \frac{\varepsilon(\lambda)}{\lambda^5} [\exp(hc/\lambda kT) - 1]^{-1} \mathrm{d}\lambda}{\int_0^\infty \eta_j(\lambda) \frac{\varepsilon(\lambda)}{\lambda^5} [\exp(hc/\lambda kT) - 1]^{-1} \mathrm{d}\lambda},$$

The calculated colour ratios may be checked against experimental observations of a hot thermocouple. Often, there is close, but not complete agreement. This may be because of inaccuracies in the data provided by the respective manufacturers for the quantum efficiency of the camera and wavelength dependent filter transmission, or simply because the optical properties of some components are unknown (for example, the camera lens). For this reason, Eq. 4 is modified to include a constant-valued scaling parameter for each colour channel, and the value of the scaling parameters is adjusted until good agreement

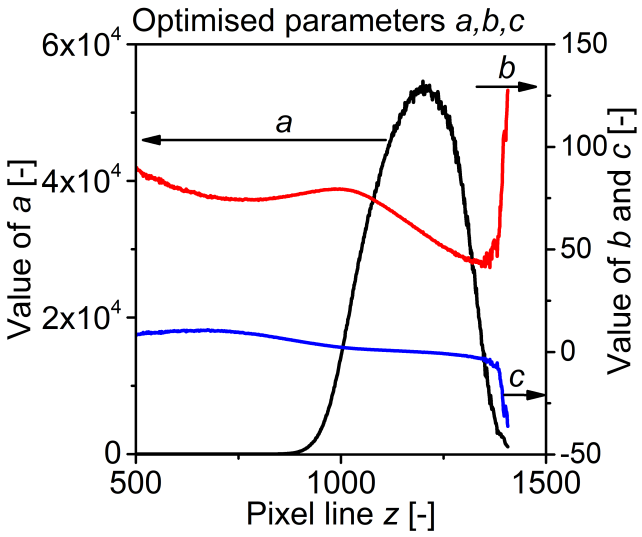

Figure S3: *Optimised fitting parameters a, b, c for the green colour channel as function of pixel row z.*

is achieved between the calculated and experimentally observed colour ratios [21]. In this work, the calibration was performed using an R-Type thermocouple and Eq. 4 was evaluated using an emissivity reported for similar thermocouples [24].

The colour ratios of the hot soot was calculated by evaluating Eq. 4 using the emissivity of soot (see the main text) and the calibrated RGB scaling parameters. The colour ratios are shown graphically in Fig. S4.

Absolute light calibration

The soot volume fraction can be calculated by evaluating Eq. 5 of the main manuscript:

$$f_\mathrm{v} \approx \frac{\lambda_\mathrm{eff}\varepsilon_\mathrm{L}}{K_\mathrm{ext}L}\frac{R_\mathrm{i}}{S_\mathrm{L}}$$

In order to evaluate this equation, it is necessary to know S_L, the light intensity of the calibration source at the same temperature as the soot. This was measured in terms of the camera response per unit exposure time for images of a thermocouple at different temperatures. See Fig. S5. All other parameters are explained in the main text.

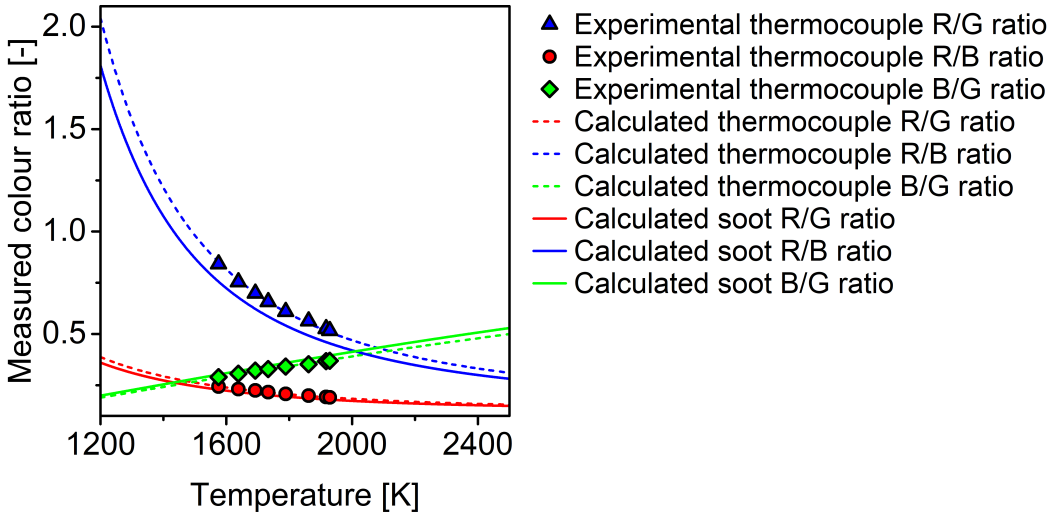

Figure S4: *Colour ratios of a hot thermocouple imaged by a camera (symbols) compared to the theoretically expected colour ratio signal expected from a thermocouple (dashed lines) and soot (solid lines).*

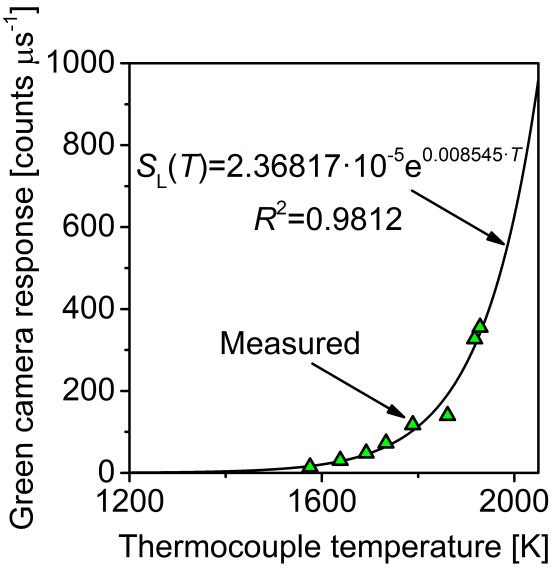

Figure S5: *Green light intensity recorded by the camera as a function of the thermocouple temperature and exponential fit used to obtain the calibration source intensity at the soot temperature S_L (see text).*